Blazar monitoring with KAT-7: PKS1510-089 a test case

N. Oozeer[1,2,3], T. Mauch[1], and R. Booth[1]

[1] SKA South Africa, The Park, Park Road, Pinelands, Cape Town 7405, South Africa
e-mail: nadeem@ska.ac.za
[2] African Institute for Mathematical Sciences, 6-8 Melrose Road, Muizenberg 7945, South Africa
[3] Centre for Space Research, North-West University, Potchefstroom 2520, South Africa

Abstract. PKS 1510-089 is a very well observed blazar with data spanning over 70 years at various wavelengths. On 2011, October 20, the blazar showed an increase in gamma-ray flux from the Fermi Gamma Ray Space telescope. We started a monitoring campaign of PKS 1510-089 on the 21st Oct 2011 until mid 2013 using the KAT-7 at 1822 MHz. We present some preliminary results from the KAT-7 science commissioning observations and detected variability in the source of the order of 46%. We furthermore detected a possible flaring in the source around MJD 56240.

Key words. galaxies: active – radio continuum: galaxies.

1. Introduction

Blazars are the most extreme class of active galactic nuclei (AGN), with relativistic jets oriented close to the line of sight of the observer. These show strong non-thermal emission across the whole band of the electromagnetic spectrum caused by relativistic beaming. Significant progress has been made in blazar physics since their detection in the γ rays by EGRET (Hartman et al. 1999). Blazars come in two subgroups, either flat-spectrum radio quasars or BL Lacerate objects, which have a featureless optical spectrum. Furthermore, they exhibit extreme variability at all wavelengths.

Variability studies across all wavelengths are crucial in understanding the physics of the central engine of AGN, which are usually too compact to be resolved with existing instruments. Their variability properties depend on the observing wavelength and can change remarkably on time-scales ranging from minutes to years. AGN variability is thought to be related to both intrinsic properties of the central engine, presumably resulting from its compactness and also to extrinsic phenomena such as the inhomogenity of the interstellar medium (ISM) through which the electromagnetic radiation propogates. Heeschen et al. (1987) found two modes of variability in compact AGN, a weak component caused by refractive interstellar scintillation and a stronger component which may be caused by intrinsic variability or further scintillation from particular regions of the ISM. However, in some sources, both intrinsic and extrinsic variability may occur at the same time (Mitchell et al. 1994).

PKS1510-089 is a flat spectrum radio loud quasar at a redshift of z=0.361. The source

has been extensively observed from the radio to gamma wavelengths. Marscher et al. (2010) showed a high correlation between the X-ray and radio flux variations which led them to conclude that X-rays are produced in the AGN via inverse Compton scattering of infrared photons by radio emitting electrons. They also noted the rotation of the optical polarisation vector during a 50 day period while the blazar was flaring at γ-ray and optical wavelengths. Using FERMI-LAT and AGILE, γ-ray variability was also detected on timescales of 6-12 hr and there was no clear correlation between the X-ray and γ-ray emission from the source(D'Ammando et al. 2009, 2011). Recent analysis by Saito et al. (2013) showed an isolated outburst, unresolved on a timescale of 3 hr using the FERMI data during the period September-December 2011. Radio band light curves of total flux density show short term variability ($\sim$ 10 - 30 days) of the source (Lazio et al. 2001; Aller et al. 2012; Kadota et al. 2012).

We started a campaign to observe PKS 1510-089 using the Karoo Array Telescope (KAT-7) from the 21st October 2011. The target was observed at least once a month as part of the science commissioning of the KAT-7. In this paper we present the preliminary results from the monitoring of PKS1510-089. §2 gives an overview of the KAT-7 and the observational parameters followed by the post-processing routines. The preliminary results are discussed in §3 and we finally conclude in §4.

Throughout this paper we assume a ΛCDM cosmology with $H_\circ$ = 73 km s^{-1} Mpc^{-1}, $\Omega_m = 0.27$, and $\Omega_\Lambda = 0.73$. All images and positions are in the J2000 coordinate system.

2. KAT-7 observations and processing

KAT-7 consists of 7 antennas of 12m diameter, equipped with cryogenically cooled receivers working between 1.2 GHz and 1.95 GHz. In continuum mode, 1024 channels covering a total bandwidth of 256 MHz inside the receivers frequency range are selected. PKS 1510-089

was observed at 1.822 GHz 38 times with integration times between $\sim$ 3 hrs up to 12hrs. The flux calibrators PKS J1939-6342 and 3C286 were observed for 3 minutes each every 3 hours in all the observing runs. Two phase calibrators PKS J1510-0543 and PKS J1517-2422 were selected. We checked images of them to ensure that no confusing sources with flux density > 10% of the phase calibrator could be seen within the 1° field of view of KAT-7. We observed the flux and phase calibrator for 3 min and the target source for 10 min, alternating between phase calibrator and target. Table 1 summarises the observation parameters.

The data reduction was carried out using an automated pipeline which automatically performs flagging, calibration, imaging and source finding steps. The pipeline uses PYTHON, AIPS (Fomalont 1981) and OBIT (Cotton 2013) and is modified from an OBIT based JVLA pipeline (Cotton, private communication) and produces continuum maps and source catalogues from KAT-7 data.

During the data reduction process, the data are first converted from the native (hdf5) format into AIPS format and scans at elevations < 20° are removed. The first and last timestamp in each scan are then removed and the frequencies of known geostationary satellites are flagged. Next a coarse automatic RFI flagging is done on the raw data in using a median window in both the time (in 256 channel average bins) and frequency (in 2 minute time average bins) domains to remove faint and broad-band RFI. The data are then hanning smoothed (using a 3 channel filter with weights [0.25,0.5,0.25]), this step halves the number of channels in the dataset to 512. After hanning a finer resolution automatic flagging is performed on the calibrator scans, to remove narrow spikes in the time and frequency domain before primary calibration.

The primary calibration step of the pipeline consists of calculating delay corrections then performing bandpass and flux calibration on the primary calibrator. The flux densities of the primary calibrators at 1822 MHz are derived from the Perley & Butler (2013) models, and are 13.61 Jy for PKS 1934-638 and 13.20 Jy for 3C286. Next, the amplitude and phase gains of
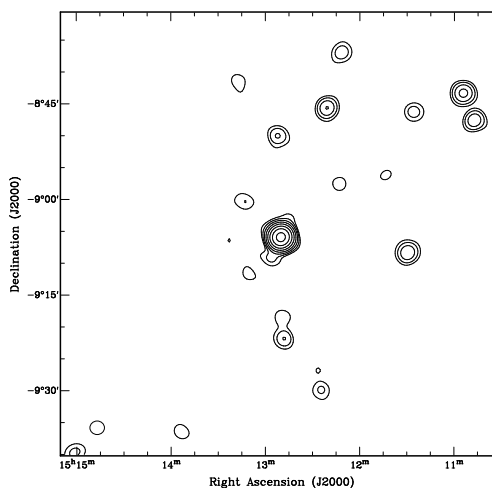
the phase calibrators are calculated and the flux density of the primary calibrator is transferred to them. The derived gains are then transferred to the target source of interest and the calibrated visibilities are flagged in time and frequency. The full first-stage calibration is run twice, with the flagging tables from the first run applied the second time around to remove any data for which the initial calibration solutions have failed.

After primary calibration the data are self-calibrated and imaged using the MFIMAGE task in Obit. Images are cleaned in a $4° \times 4°$ area centered on the target and the SUMSS and NVSS surveys are searched down to a flux limit of 50 mJy at 1822 MHz (assuming a spectral index of −0.7) out to 10° and clean boxes are placed at the positions of these sources. Imaging is done by splitting the frequency band into 9 equal sub-bands of 26.5 MHz and cleaning each of these separately, then combining the sub-bands and clean components to produce the final image. A constant resolution with frequency is made before producing the final image by convolving the residual images and clean components by the resolution of the lowest frequency sub-band. The data is subject to 3 iterations of phase-only self calibration on a 10 s solution interval to a flux limit of 25 mJy using a sky-model derived from clean components found over the image, and those found in the clean boxes derived from the SUMSS and NVSS data. Then the data is then given 2 iterations of amplitude and phase calibration on a 2 min solution interval using the clean components over the same area as for the phase-only self calibration, to a flux limit of 100 mJy.

We assume that the target source is a point source and is the brightest source in the final image and we therefore derive the flux density of the target source by interpolating pixels to the peak value in the image. The image rms (used to calulate the measured flux density error) is derived by iteratively fitting a Gaussian function to the pixel distribution in the image and rejecting pixels further than 5σ from the mean until the mean and standard deviation of the fitted Gaussian changes by 0.1 %. Flux density errors are calculated as the quadritic sum of an empirical 5 % KAT-7 calibration error

Table 1. KAT-7 Observations parameters.

Central Frequency	1822 MHz
Bandwidth	256 MHz
No. of antennas	5∼7
Min Baseline	26 m
Max Baseline	185 m
Time on target	∼4–10 hrs
Flux calibrators	3C286
	PKS 1934-638
Phase calibrators	PKS J1510-0543
	PKS J1517-2422

Fig. 1. Contours showing PKS 1510-089, observed on 22nd Feb 2012 and reduced using the pipeline described in Section 2. The contours are at [-2, 2, 4, 8, 16, 32, 64, 128, 256] $\times$ 5.8 mJy beam^{-1}. The image rms is around 1.9 mJy beam^{-1}.

(derived by examining variations in calibration solutions over a year of KAT-7 observations) and the image rms. For the bright sources discussed here, errors are dominated by the calibration term.

In Fig. 1 , we show an example image produced by the KAT-7. This observation was carried out with 6 antennas (one of the central antennas (ant4) was missing). The measured peak flux of the target in the middle of the field is 1.9687±0.099 Jy beam^{-1}. The source is unresolved with KAT-7 in all observations.
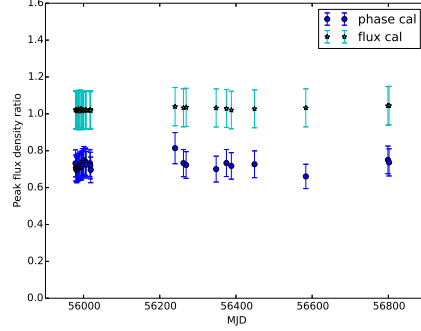
3. Analysis and results

As mentioned in Section 1, the flux density of PKS 1510-089 changes remarkably on the time-scales ranging from minutes to years over the entire electromagnetic spectrum. We have observed the source at 1822 MHz on numerous occasions over a 2 year peroid using KAT 7 to monitor this variability and to determine the feasability of future variability studies with the telescope. In this work we only accepted observations where a minimum of 6 antennas of the array were available and therefore there are missing data from Mar 2012 to Oct 2012. The final dataset comprises 38 observations of the target. Fig. 2b shows the measured flux density of PKS 1510-089 over the period.
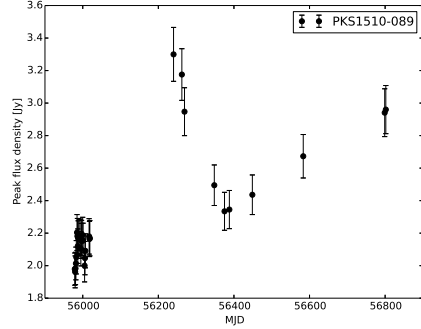
From a study by Perley & Butler (2013), 3C286 shows a variability of 1% over a span of 30 years while Tzioumis et al. (2010) mention that PKS 1934-638 is known to be very stable source. We take the ratios of the flux densities of the two flux calibrators in each observation to establish if there is any variability in the targets measured by KAT-7 over the time period, we also calculate a similar ratio for the two phase calibrators (PKS J1510-0543 & PKS J1517-2422). The flux ratio of the phase calibrators and the flux calibrators are plotted in Fig (2a). We conclude that the flux and phase calibrators show very little variation over the period studied.

In Fig. 2b, even though there is some missing data due to a lack of available KAT-7 antennas, there appears to be a flaring in PKS1510-089 around MJD 56240, which corresponds to around 11 October 2012. We also calculated the ratio of the flux density of the target PKS1510-089 with respect to the two phase calibrators. The flux ratio is seen to fluctuate between 0.824 - 1.303 with respect to PKS J1517-2422 and between 0.589 - 0.997 with respect to PKS J1510-0543. These fluctuations are much larger than those seen in Fig. 2a and indicate strong variability of PKS1510-089.

For a statistical analysis of the variability of PKS J1510-089, we use several quantities:

(a) The ratio of the peak flux density of the flux calibrators (cyan) and that of the phase calibrators (blue). The error bars are the quadratic sum of the measured flux density errors as described in Section 3.

(b) Peak flux density fluctuations of PKS1510-089 over span of 2 years. Error bars are as described in Section 3. A possible flare is seen around MJD 56240.

Fig. 2. The variability of the calibrators and the target over the course of the observations.

3.1. Reduced Chi-Square

In order to test the variability, we assume a null hypothesis (H_0) implying a source has a constant (non-variable) flux density. The reduced Chi-Square, (χ_r^2) defined as:

$$\chi_r^2 = \frac{1}{N-1} \sum \left(\frac{S_i - \langle S \rangle}{\Delta S_i} \right)^2 \tag{1}$$

was used as a first approximation to check the variability of the sources. Here the S_i are individual flux-density measurements for the tar-

Table 2. Various derived statistical parameters.

Source	χ^2	V_{rms} %	MI %	$Y_{[3C286]}$ %	$Y_{[PKS\,1934]}$ %
3C286	0.023	-4.979	0.746	-	-1.746
PKS 1934-638	0.009	-4.946	0.467	1.746	-
PKS J1510-0543	0.124	-4.000	1.713	4.625	4.944
PKS J1517-2422	0.542	-4.700	3.694	10.854	10.994
PKS 1510-089	7.434	14.713	15.559	46.624	46.657

get, ΔS_i is the error on each measurement respectively, N is the number of data points and $\langle S \rangle$ is the mean flux density. Sources are considered variable if they have $\chi_r^2 > 6.6$, corresponding to a probability of $\leq 0.1\%$ for the null hypothesis.

3.2. Variability index (V_{rms})

Aller (1999) defined the variability index as the ratio of the difference between the maximum and minimum flux density to the sums of these two quantities. This is useful to understand the maximum observed fractional variation but on the other hand uses only two points of the entire datasets, which is biased by the presence of outliers. Following Sadler et al. (2006), we computed an alternative form of the variability index, which takes into account all of the individual flux densities and their uncertainties as follows:

$$V_{rms} = \frac{100}{\langle S \rangle} \sqrt{\frac{\sum [S_i - \langle S \rangle]^2 - \sum \Delta S_i^2}{N}}. \qquad (2)$$

We used a distribution of positive and negative V_{rms} rather than setting the V_{rms} to be zero when the square root in Equ. 2 becomes negative. Sadler et al. (2006) indicated that a source was variable if its V_{rms} value was greater than 6%.

3.3. The modulation index

The modulation index provides a measure of strength of the observed amplitude variations

without taking account of the error of the individual measurement. We define the modulation index MI (Kraus et al. 2003) as follows:

$$MI = 100 \times \frac{2\sigma_I}{\langle S \rangle} \qquad (3)$$

where σ_I is the standard deviation. This is the equivalent of the normalised standard deviation. The amplitude variability for a source is then given by:

$$Y = 3 \sqrt{MI^2 - MI_0^2} \qquad (4)$$

where MI_0 is the modulation index of the non-variable sources, in our case the flux calibrators 3C286 or PKS 1934-638. The Y value has the advantage that it is a comparison of the source with targets that are assumed to be non variable (i.e. the flux calibrators).

The various statistical parameters for all the sources are shown in Table 2, PKS 1510-089 shows considerable variability in all measures tested, the calibrator sources show little to no variability.

4. Conclusions

In order to investigate the variability of the blazar PKS 1510-089, we have used several statistical metrics as described in § 3. We noticed that the source does show variability in the radio at 1822 MHz as measured by the KAT-7, with a modulation index $\sim$ 16% and a Y factor of 46 %. We also detected a strong increase in the flux of PKS1510-089 around MJD 56240 which can be due to flaring. We

have assumed that the the 'core' of the blazar is the only component small enough in angular size to scintillate. From VLBI observations of a sample of BL Lac objects, Bach et al. (2006) have found that jet features (steep spectrum) do become as bright as, or even brighter than, the core itself at high frequency. Any core fluctuations in the flat spectrum source, will be readily measurable as compared to fluctuations in steep spectrum sources.

This variability in PKS1510-089 has also been previously measured at other wavelengths. At this frequency ∼ 1GHz, one might expect both intrinsic and extrinsic variability from the source. In order to confirm this variability is explicitly of intrinsic nature, we have started a multi-wavelength followup with other radio telescope. Through a more detailed analysis, useful constraints on the variability of this source may be provided.

References

Aller, M. F. 1999, BL Lac Phenomenon, 159, 31

Aller, M. F., Aller, H. D., Hughes, P. A., et al. 2012, American Astronomical Society Meeting Abstracts #220, 220, #335.01

Bach, U., Villata, M., Raiteri, C. M., et al. 2006, A&A, 456, 105

Cotton, B. 2013, Astrophysics Source Code Library, 7008

D'Ammando, F., Raiteri, C. M., Villata, M., et al. 2011, A&A, 529, A145

D'Ammando, F., Pucella, G., Raiteri, C. M., et al. 2009, A&A, 508, 181

Fomalont, E. 1981, National Radio Astronomy Observatory Newsletter, 3, 3

Hartman, R. C., Bertsch, D. L., Bloom, S. D., et al. 1999, ApJS, 123, 79

Heeschen, D. S., et al. 1987, AJ, 94, 1493

Kadota, A., et al. 2012, PASJ, 64, 109

Kraus, A., Krichbaum, T. P., Wegner, R., et al. 2003, A&A, 401, 161

Lazio, T. J. W., Waltman, E. B., Ghigo, F. D., et al. 2001, ApJS, 136, 265

Marscher, A. P., Jorstad, S. G., Larionov, V. M., et al. 2010, ApJ, 710, L126

Mitchell, K. J., Dennison, B., Condon, J. J., et al. 1994, ApJS, 93, 441

Perley, R. A., & Butler, B. J. 2013, ApJS, 204, 19

Sadler, E. M., Ricci, R., Ekers, R. D., et al. 2006, MNRAS, 371, 898

Saito, S., Stawarz, Ł., Tanaka, Y. T., et al. 2013, ApJ, 766, L11

Tzioumis, A. K., Tingay, S. J., Stansby, B., et al. 2010, AJ, 140, 1506

Ulrich, M.-H., Maraschi, L., & Urry, C. M. 1997, ARA&A, 35, 445